Self-Assembly of Molecular Brick Wall and Molecular Honeycomb from Nickel(II) Macrocycle and 1,3,5-Benzenetricarboxylate: Guest-Dependent Host Structures

Hye Jin Choi and Myunghyun Paik Suh*

Contribution from the Department of Chemistry Education and The Center for Molecular Catalysis, Seoul National University, Seoul 151-742, Republic of Korea

Received February 16, 1998

Abstract: Novel multidimensional supramolecular networks with brick wall and honeycomb structures, $[Ni(C_{12}H_{30}N_6O_2)]_3[C_6H_3(COO)_3]_2 \cdot 18H_2O$ (**1**) and $[Ni(C_{12}H_{30}N_6O_2)]_3[C_6H_3(COO)_3]_2 \cdot 14H_2O \cdot 2C_5H_5N$ (**2**), respectively, have been constructed by the self-assembly of $S = 0$ Ni(II) macrocyclic complex containing hydroxyl pendent chains and 1,3,5-benzenetricarboxylate (BTC^{3-}). The host structures assembled are greatly affected even by the partial change of the guests. X-ray crystal structures indicate that each Ni(II) macrocycle binds two BTC^{3-} in the trans position and each BTC^{3-} coordinates three Ni(II) macrocyclic units via C_1 symmetry in **1** and C_3 symmetry in **2**. The simplest cyclic motif of the two-dimensional (2-D) networks in **1** and **2** is a large ring consisting of six Ni(II) macrocyclic complexes and six BTC^{3-} anions. The rings are extended to form a 2-D layer. The layers are stacked in parallel, separated by 8.850 Å in **1** and 8.973 Å in **2**. They are interconnected by the hydrogen-bonding interactions between the hydroxyl pendants of the macrocycle in a layer and the secondary amines of the macrocycle located in the neighboring layers, which gives rise to the three-dimensional structures. The effective cavity size of **1** is ca. 6.7 × 13 Å and that of **2** ca. 11.4 × 11.4 Å. The cavities are filled with guest molecules. In **2**, the pyridine guest experiences $\pi-\pi$ interaction with the benzene ring of BTC^{3-}. Variable-temperature (2−300 K) magnetic susceptibility measurements indicate that both **1** and **2** exhibit weak anti-ferromagnetic interactions between the $S = 1$ Ni(II) paramagnetic centers.

Introduction

Self-assembled infinite metal complexes with specific network topologies attract great attention due to their potential properties as functional solid materials as well as fascinating molecular structures.[1−19] Especially, the assembly of organic molecules and metal-ion building blocks may yield a new generation of multidimensional networks which contain channels or cavities of various sizes and shapes.[16−26] In addition, the assembly can provide highly ordered multidimensional networks containing

(1) (a) Bein, T. *Supramolecular Architecture*: *Synthetic Control in Thin Films and Solids*; ACS Symposium Series 499; American Chemical Society: Washington, DC, 1992; Chapter 19. (b) Amabilino, D. B.; Stoddart, J. F. *Chem. Rev.* **1995**, *95*, 2725. (c) Whitesides, G. M. *Sci. Am.* **1995**, 114. (d) Lehn, J.-M. *Supramolecular Chemistry*: *Concepts and Perspectives*; VCH Publishers: Weinheim, Germany, 1995. (d) Lawrence, D. S.; Jiang, T.; Levett, M. *Chem. Rev.* **1995**, *95*, 2229. (e) Iwamoto, T. *Inclusion Compounds*; Atwood, J. L., Davies, J. E. D., MacNicol, D. D., Eds.; Academic Press: London, 1991; Vol. 5, Chapter 6, pp 177−212.

(2) Bhyrappa, P.; Wilson, S. R.; Suslick, K. S. *J. Am. Chem. Soc.* **1997**, *119*, 8492.

(3) Lu, J.; Paliwala, T.; Lim, S. C.; Yu, C.; Niu, T.; Jacobson, A. J. *Inorg. Chem.* **1997**, *36*, 923.

(4) Huck, W. T. S.; Hulst, R.; Timmerman, P.; Veggel, F. C.; Reinhoudt, D. N. *Angew. Chem., Int. Ed. Engl.* **1997**, *36*, 1006.

(5) Fujita, M.; Aoyagi, M.; Ibukuro, F.; Ogura, K.; Yamaguchi, K. *J. Am. Chem. Soc.* **1998**, *120*, 611.

(6) Stang, P. J.; Persky, N. E.; Manna, J. *J. Am. Chem. Soc.* **1997**, *119*, 4777.

(7) Gardner, G. B.; Venkataraman, D.; Moore, J. S.; Lee, S. *Nature* **1995,** *374*, 792.

(8) Hartgerink, J. D.; Granja, J. R.; Milligan, R. A.; Ghadiri, M. R. *J. Am. Chem. Soc.* **1996**, *118*, 43.

(9) Ashton, P. R.; Collins, A. N.; Fyfe, M. C. T.; Menzer, S.; Stoddart, J. F.; Williams, D. J. *Angew. Chem., Int. Ed. Engl.* **1997**, *36*, 735.

(10) Janiak, C. *Angew. Chem., Int. Ed. Engl.* **1997**, *36*, 1431.

(11) Real, J. A.; Andrés, E.; Muñoz, M. C.; Julve, M.; Granier, T.; Bousseksou, A.; Varret, F. *Science* **1995**, *268*, 265.

(12) Stumpf, H. O.; Ouahab, L.; Pei, Y.; Grandjean, D.; Kahn, O. *Science* **1993,** *261,* 447.

(13) Fujita, M.; Yoon, J. K.; Sasaki, O.; Yamaguchi, K.; Ogura, K. *J. Am. Chem. Soc.* **1995**, *117*, 7287.

(14) Whiteford, J. A.; Lu, C. V.; Stang, P. J. *J. Am. Chem. Soc.* **1997**, *119*, 2524.

(15) Batten, S. R.; Hoskins, B. F.; Robson, R. *J. Am. Chem. Soc.* **1995**, *117*, 5385.

(16) Yaghi, O. M.; Li, H.; Groy, T. L. *J. Am. Chem. Soc.* **1996**, *118*, 9096.

(17) Subramanian, S.; Zaworotko, M. J. *Angew. Chem., Int. Ed. Engl.* **1995**, *34*, 2127.

(18) Hennigart, T. L.; Macquarrie, D. C.; Losier, P.; Rogers, R. D.; Zaworotko, M. J. *Angew. Chem., Int. Ed. Engl.* **1997**, *36*, 972.

(19) Yaghi, O. M. In *Access in Nanoporous Materials*; Pinnavania, T. L., Thorpe, M. F., Eds.; Plenum: New York, 1995; p 111.

(20) (a) Yaghi, O. M.; Davis, C. E.; Li, G.; Li, H. *J. Am. Chem. Soc.* **1997**, *119*, 2861. (b) Yaghi, O. M.; Li, H. *J. Am. Chem. Soc.* **1995**, *117*, 10401. (c) Yaghi, O. M.; Li, G.; Li, H. *Nature* **1995**, *378*, 703. (d) Yaghi, O. M.; Sun, Z.; Richardson, D. A.; Groy, T. L. *J. Am. Chem. Soc.* **1994**, *116*, 807. (e) Yaghi, O. M.; Jernigan, R.; Li, H.; Davis, C. E.; Groy, T. L. *J. Chem. Soc., Dalton Trans.* **1997**, 2383.

(21) (a) Abrahams, B. F.; Hoskins, B. F.; Liu, J.; Robson, R. *J. Am. Chem. Soc.* **1991**, *113*, 3045. (b) Abrahams, B. F.; Hoskins, B. F.; Robson, R. *J. Chem. Soc., Chem. Commun.* **1990**, 60.

(22) Harrison, W. T. A.; Hannooman, L. *Angew. Chem., Int. Ed. Engl.* **1997**, *36*, 640.

(23) Venkataraman, D.; Gardner, G. B.; Lee, S.; Moore, J. S. *J. Am. Chem. Soc.* **1995**, *117*, 11600.

(24) Kondo, M.; Yoshitomi, T.; Seki, K.; Matsuzaka, H.; Kitagawa, S. *Angew. Chem., Int. Ed. Engl.* **1997**, *36*, 1725.

(25) Hoskins, B. F.; Robson, R.; Slizys, D. A. *J. Am. Chem. Soc.* **1997**, *119*, 2952.

(26) Carlucci, L.; Ciani, G.; Proserpio, D. M.; Sironi, A. *J. Am. Chem. Soc.* **1995**, *117*, 4562.

10.1021/ja980504l CCC: $15.00
Published on Web 10/06/1998

Scheme 1

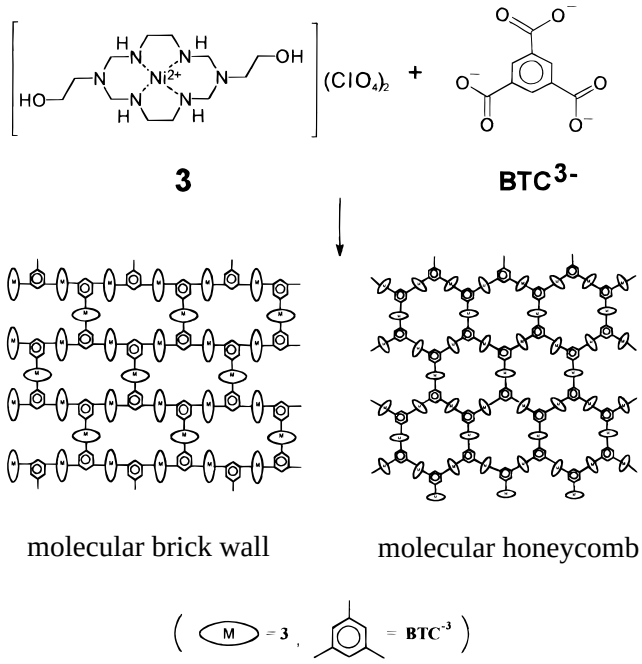

many paramagnetic metal centers that can give insight into the magnetostructural relationship which plays a key role in the development of molecular magnetic materials.[12]

Here, we report novel molecular brick wall (pattern *a*) and molecular honeycomb (pattern *b*) containing many paramagnetic

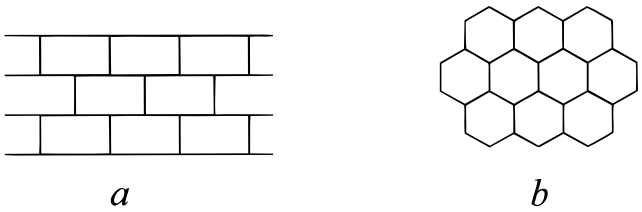

Ni(II) centers, $[Ni(C_{12}H_{30}N_6O_2)]_3[C_6H_3(COO)_3]_2 \cdot 18H_2O$ (**1**) and $[Ni(C_{12}H_{30}N_6O_2)]_3[C_6H_3(COO)_3]_2 \cdot 14H_2O \cdot 2C_5H_5N$ (**2**), respectively, which are self-assembled by square-planar Ni(II) macrocyclic complex (**3**) and 1,3,5-benzenetricarboxylate (BTC^{3-}) as depicted in Scheme 1. Host topologies of the supramolecular networks depend on the partial change of the guest molecules.

Our synthetic strategy was to construct the two-dimensional (2-D) networks with big honeycomb-like structures based on alternating BTC^{3-} and macrocyclic complex and then stack the 2-D sheets together through the interlayer hydrogen bonds to create channels. To build the desired molecular architecture, each carboxylate of BTC^{3-} should bind a metal ion in monodentate fashion, although it can act as monodentate or bidentate depending upon the coordination environment of metal ion.[16,20,27] In addition, each metal should bind two BTC^{3-} in the trans position. To stack the layers, macrocycles should contain functional groups that can be involved in the hydrogen bonding. Considering these requirements, we chose the square-planar Ni(II) complex of macrocycle containing hydroxyl pendants, **3**,[28] as a metal building block.

Experimental Section

General. Infrared spectra were recorded with a Perkin-Elmer 2000 FT-IR spectrophotometer. Elemental analyses were performed by the analytical laboratory of Seoul National University. UV/vis diffuse reflectance spectra were recorded with a Cary 300 Bio UV/vis spectrophotometer. Magnetic susceptibility was measured in the temperature range of 2−300 K at 0.5 T on a Quantum Design MPMS superconducting quantum interference device (SQUID). Thermogravimetric analysis (TGA) and differential thermal analysis (DTA) were performed at a scan rate of 3 °C/min using a Rigaku Tas-100 system. X-ray powder diffraction data were recorded on a MAC Science M18XHF-22 diffractometer at 50 kV and 100 mA for Cu Kα (λ = 1.5406 Å) with a scan speed of 5 deg/min and a step size of 0.02° in 2θ.

$[Ni(C_{12}H_{30}N_6O_2)](ClO_4)_2$. The macrocyclic compound was prepared according to the literature procedures previously reported.[28]

Na_3BTC. To a stirred aqueous suspension (25 mL) of 1,3,5-benzenetricarboxylic acid (2.12 g, 0.01 mol) was added an aqueous solution of NaOH (1.55 g, 0.04 mol). The solution was filtered and concentrated until white precipitate started to form, and ethanol (20 mL) was added. The solution was allowed to stand in a refrigerator for several hours. White precipitate formed was filtered off, washed with ethanol, and dried in vacuo. Yield: 95%. IR (Nujol mull): ν_{COO^-}, 1620, 1368 cm^{-1}.

$[Ni(C_{12}H_{30}N_6O_2)]_3[C_6H_3(COO)_3]_2 \cdot 18H_2O$ (1). A DMF solution (12 mL) of $[Ni(C_{12}H_{30}N_6O_2)](ClO_4)_2$ (0.5 g, 0.91 mmol) was allowed to diffuse into an aqueous solution (2 mL) of Na_3BTC (0.17 g, 0.62 mmol) in a tube for several days. Large pale purple crystals formed at the water/DMF interface, which were collected by filtration under water vapor. Yield: ca. 80%. The compound loses some of the water guests upon exposure to the atmosphere. Anal. Calcd for the anhydrous sample obtained by heating **1** at 120 °C for 2 h, $[Ni(C_{12}H_{30}N_6O_2)]_3[C_6H_3(COO)_3]_2$ ($Ni_3C_{54}H_{96}N_{18}O_{18}$): C, 44.38; H, 6.62; N, 17.25. Found: C, 44.00; H, 6.55; N, 16.95. FT-IR (Nujol mull): 3359 (br), 3263 (s), 3158 (s), 1608 (s), 1563 (s), 1431 (s), 1361 (s), 1259 (m), 1275 (m), 1239 (w), 1149 (w), 1059 (m), 1024 (s), 955 (m), 930 (m), 883 (w), 855 (w), 768 (m), and 718 (s) cm^{-1}. UV/vis (diffuse reflectance spectrum, λ_{max}): 504 and 652 nm.

$[Ni(C_{12}H_{30}N_6O_2)]_3[C_6H_3(COO)_3]_2 \cdot 14H_2O \cdot 2C_5H_5N$ (2). Method 1. **$[Ni(C_{12}H_{30}N_6O_2)](ClO_4)_2$** (0.12 g, 0.22 mmol) was dissolved in the mixture of DMF (1 mL) and pyridine (1 mL), and then the aqueous solution (1.6 mL) of Na_3BTC (0.051 g, 0.18 mmol) was added dropwise. To the resulting purple solution was added pyridine (0.5 mL) additionally to induce crystallization of the product, and then the solution was allowed to stand in a refrigerator for 2 days. Pale purple crystals formed were filtered and washed briefly with ethyl ether. Yield: ca. 20%. **Method 2.** The molecular brick wall **1** (0.055 g) was dissolved in a minimum amount (0.5 mL) of water, and pyridine (3 mL) was added. The solution was allowed to stand at room temperature for several hours until pale purple crystals formed. The crystals were filtered off and washed briefly with ethyl ether. Yield: ca. 60%. Anal. Calcd for $Ni_3C_{64}H_{134}N_{20}O_{32}$: C, 41.06; H, 7.22; N, 14.96. Found: C, 42.60; H, 7.17; N, 16.01. FT-IR (Nujol mull): 3356 (br), 3260 (s), 3161 (s), 1609 (s), 1565 (s), 1430 (s), 1355 (s), 1262 (m), 1169 (w), 1149 (w), 1062 (m), 1026 (s), 953 (m), 928 (m), 880 (w), 800 (w), 771 (m), and 715 (s) cm^{-1}. UV/vis (diffuse reflectance spectrum, λ_{max}): 505 and 647 nm.

X-ray Diffraction Measurements. The single crystals of **1** and **2** were sealed in the glass capillaries containing their mother liquor. The X-ray data were collected at room temperature using graphite monochromated Mo Kα radiation on an Enraf-Nonius CAD4 for **1** and Siemens CCD diffractometer for **2**. The orientation matrix and unit cell parameters were determined from 25 machine-centered reflections with $16° < 2\theta < 25°$. Axial photographs were used to verify the unit cell choice. Data were corrected for Lorentz and polarization effects. Absorption correction was not made for **1,** but it was made for **2**. All calculations were carried out on a personal computer with use of SHELXS-86[29] and SHELXL-93[30] programs. The structures were solved by the direct method. All non-hydrogen atoms were refined anisotropically. All hydrogen atoms were positioned geometrically and refined using a riding model. In **1,** the hydroxyl pendants uninvolved in the

(27) Smith, G.; Reddy, A. N.; Byriel, K. A.; Kennard, C. H. L. *J. Chem. Soc., Dalton Trans*. **1995**, 3565.

(28) Suh, M. P.; Shim, B. Y.; Yoon, T. S. *Inorg. Chem.* **1994**, *33*, 5509.

(29) Sheldrick, G. M. *Acta Crystallogr*. **1990**, *A46*, 467.

(30) Sheldrick, G. M. *SHELXL93, Program for the Refinement of Crystal Structures*; University of Göttingen: Göttingen, Germany, 1993.

Table 1. Crystallographic Data for $[Ni(C_{12}H_{30}N_6O_2)]_3[C_6H_3(COO)_3]_2\cdot 18H_2O$ (**1**) and $[Ni(C_{12}H_{30}N_6O_2)]_3[C_6H_3(COO)_3]_2\cdot 14H_2O\cdot 2C_5H_5N$ (**2**)

	1	**2**
formula	$Ni_3C_{54}H_{132}N_{18}O_{36}$	$Ni_3C_{64}H_{134}N_{20}O_{32}$
fw	1785.9	1872.04
crystal system	triclinic	triclinic
space group	$P\bar{1}$	$P\bar{1}$
a, Å	9.7920(10)	9.9520(6)
b, Å	15.474(3)	16.7476(10)
c, Å	16.846(3)	18.8263(11)
α, deg	93.210(10)	113.4120(10)
β, deg	93.250(10)	97.5100(10)
γ, deg	103.230(10)	94.5240(10)
Z, formula unit	1	1
V, Å^3	2474.5(7)	2825.1(3)
d_{calcd}, g·cm^{-3}	1.198	1.10
μ_{calcd}, mm^{-1}	0.644	0.565
no. of data collcd	9373	11755
no. of unique data (all)	8690	7848
no. of obsd data [$F > 4(\sigma F)$]	4609	4387
no. of variable params	509	544
R_1,[a] wR_2[b] (4σ)	0.0782, 0.1887	0.0944, 0.2180
R_1,[a] wR_2[b] (all data)	0.1514, 0.2782	0.1773, 0.3287
gof (all data)	0.9095	1.042

[a] $R = \sum||F_o| - |F_c||/\sum|F_o|$. [b] $wR(F^2) = [\sum w(F_o^2 - F_c^2)^2/\sum w(F_o^2)^2]^{1/2}$. $w = 1/[\sigma^2(F_o^2) + (0.1309P)^2 + 0.0000P]$, where $P = (F_o^2 + 2F_c^2)/3$ for **1**. $w = 1/[\sigma^2(F_o^2) + (0.1563P)^2 + 0.0000P]$, where $P = (F_o^2 + 2F_c^2)/3$ for **2**.

Table 2. Selected Bond Distances (Å) and Angles (deg) for $[Ni(C_{12}H_{30}N_6O_2)]_3[C_6H_3(COO)_3]_2\cdot 18H_2O$ (**1**)[a]

Ni1−N1A	2.057(5)	Ni3−O5	2.152(4)
Ni1−N2A	2.053(5)	O1−C7	1.260(7)
Ni1−O1	2.149(4)	O2−C7	1.260(7)
Ni2−N1B	2.043(5)	O3−C8	1.257(7)
Ni2−N2B	2.049(5)	O4−C8	1.250(8)
Ni2−O3	2.140(4)	O5−C9	1.257(8)
Ni3−N1C	2.056(7)	O6−C9	1.227(8)
Ni3−N2C	2.061(6)		
N2A−Ni1−N1A′	93.9(2)	C9−O5−Ni3	132.9(4)
N1A−Ni1−O1′	92.7(2)	O1−C7−O2	124.3(7)
N2A−Ni1−O1′	88.1(2)	O1−C7−C10	117.9(5)
N1B−Ni2−N2B″	86.2(2)	O2−C7−C10	117.5(5)
N1B−Ni2−O3″	92.3(3)	O3−C8−O4	125.1(6)
N2B−Ni2−O3″	89.6(2)	O3−C8−C12	117.1(6)
N2C−Ni3−O5‴	87.6(2)	O4−C8−C12	117.8(6)
N1C−Ni3−O5‴	86.9(2)	O6−C9−O5	125.4(6)
N2C−Ni3−N1C‴	93.6(3)	O6−C9−C14	118.1(6)
C7−O1−Ni1	135.6(4)	O5−C9−C14	116.4(6)
C8−O3−Ni2	133.8(4)		

[a] Symmetry transformations used to generate equivalent atoms: prime, $-x$, $-y$, $-z$; double prime, $-x-1$, $-y$, $-z+1$; triple prime, $-x-1$, $-y-1$, $-z$.

hydrogen bonding (O1B, O1C, and C6B) as well as some of the guest water molecules (OW2, OW6, and OW8) experience the thermal disorder. In **2**, the hydroxyl pendants (O1A, O1B, O1C, C6B, and C6C), included pyridine (N1 and C1−C5) and some guest water molecules (OW5, OW6, and OW7) experience the thermal disorder. The crystallographic data of **1** and **2** are summarized in Table 1 and the selected bond distances and angles in Tables 2 and 3.

Guest Inclusion Experiments in Molecular Brick Wall 1. A few milligrams of freshly prepared pink crystals of **1** were immersed in solvents such as benzene, toluene, pyridine, DMF, and benzyl alcohol for 12 h at room temperature and then filtered. For the resulting solid, the morphology was examined under the microscope and the elemental analysis was carried out.

Results and Discussion

Self-Assembly. The assembly of honeycomb-like structure is challenging since the hexagon represents the most common pattern in nature[31] and is familiar from benzene to the honeycomb of the bee. Honeycomb-like networks have been previously obtained for $[Ag(TCB)(CF_3SO_3)]$,[7] where TCB represents 1,3,5-tricyanobenzene and $Cd(CN)_2\cdot{}^2/_3H_2O\cdot Bu^tOH$.[21]

The self-assembly from square-planar Ni(II) macrocyclic complex **3** and BTC^{3-} salt in water−DMF resulted in a molecular brick wall **1** instead of honeycomb-like structure. However, the similar self-assembly in the presence of pyridine or the reassembling of **1** in water in the presence of excess amount of pyridine resulted in the molecular honeycomb **2**. The different molecular topologies in **1** and **2** arose from the different coordination mode of BTC^{3-} anion. BTC^{3-} coordinates metal ions via C_1 symmetry in **1**, while it coordinates metal ions via C_3 rotational symmetry in **2**. The symmetrical binding mode of BTC^{3-} in **2** seems to be induced by the $\pi-\pi$ interaction between the included pyridine molecule and the benzene rings of BTC^{3-} anions of the host layers, as will be discussed in the later part of this paper. In both **1** and **2**, the hydroxyl pendants of the macrocycle involve in the hydrogen bonding to interconnect the 2-D sheets, as revealed by the X-ray diffraction analysis. When Ni(II) cyclam ($C_{10}H_{24}N_4$), the macrocycle without polar side chains, was used as a metal building block, a completely different supramolecular network was constructed.[32]

Table 3. Selected Bond Distances (Å) and Angles (deg) for $[Ni(C_{12}H_{30}N_6O_2)]_3[C_6H_3(COO)_3]_2\cdot 14H_2O\cdot 2C_5H_5N$ (**2**)[a]

Ni1−N1A	2.062(6)	Ni3−O5	2.115(5)
Ni1−N2A	2.056(6)	O1−C7	1.242(9)
Ni1−O1	2.139(5)	O2−C7	1.272(9)
Ni2−N1B	2.051(6)	O3−C8	1.266(9)
Ni2−N2B	2.059(7)	O4−C8	1.237(9)
Ni2−O3	2.143(5)	O5−C9	1.264(9)
Ni3−N1C	2.065(8)	O6‴−C9	1.248(9)
Ni3−N2C	2.037(6)		
N1A−Ni1−N2A	85.0(3)	C8−O3−Ni2	134.0(5)
N1A−Ni1−O1′	87.2(2)	C9−O5−Ni3	137.5(5)
N2A−Ni1−O1′	87.6(2)	O1−C7−O2	124.9(7)
N1B−Ni2−N2B	94.3(3)	O1−C7−C10	116.8(7)
N2B−Ni2−O3	86.8(3)	O2−C7−C10	118.2(6)
N1B−Ni2−O3	93.4(2)	O3−C8−O4	124.3(7)
N2C−Ni3−N1C	85.7(3)	O3−C8−C12	116.7(7)
N2C−Ni3−O5	87.8(2)	O4−C8−C12	119.0(7)
N1C−Ni3−O5	87.9(3)	O6‴−C9−C14	119.2(7)
O5−C9−C14	116.0(7)	O6‴−C9−O5	124.7(7)
C7−O1−Ni1	137.2(5)		

[a] Symmetry transformations used to generate equivalent atoms: prime, $-x+1$, $-y+1$, $-z$; double prime, $-x+2$, $-y+1$, $-z+1$; triple prime, $-x+2$, $-y$, $-z$.

X-ray Crystal Structure of Molecular Brick Wall 1. The X-ray crystal structure of the fundamental building unit of **1** is shown in Figure 1a. The coordination geometry around Ni(II) ion is a tetragonally distorted octahedron in which Ni(II) ion is coordinated by four secondary nitrogen donors of the macrocycle and by two carboxylate oxygen atoms of BTC^{3-} ions. The average Ni−N and Ni−O bond distances are 2.054(2) and 2.147(2) Å, respectively. Each BTC^{3-} coordinates three Ni(II) macrocyclic units through C_1 symmetry instead of C_3 rotational symmetry and the metal−metal distances around BTC^{3-} are asymmetric: Ni1- - -Ni3 = 8.154(1), Ni1- - -Ni2 = 9.980(2), and Ni2- - -Ni3 = 11.113(2) Å. The dihedral angles between the benzene plane of BTC^{3-} and three macrocyclic coordination planes involving Ni1, Ni2, and Ni3 are 85.3(2), 71.4(2), and 81.1(2)°, respectively. The simplest cyclic motif of the 2-D network is a large 48-membered rectangular ring consisting of six Ni(II) macrocyclic complexes and six BTC^{3-},

(31) Ozin, G. A. *Acc. Chem. Res.* **1997**, *30*, 17.
(32) Choi, H. J.; Suh, M. P. Submitted for publication.

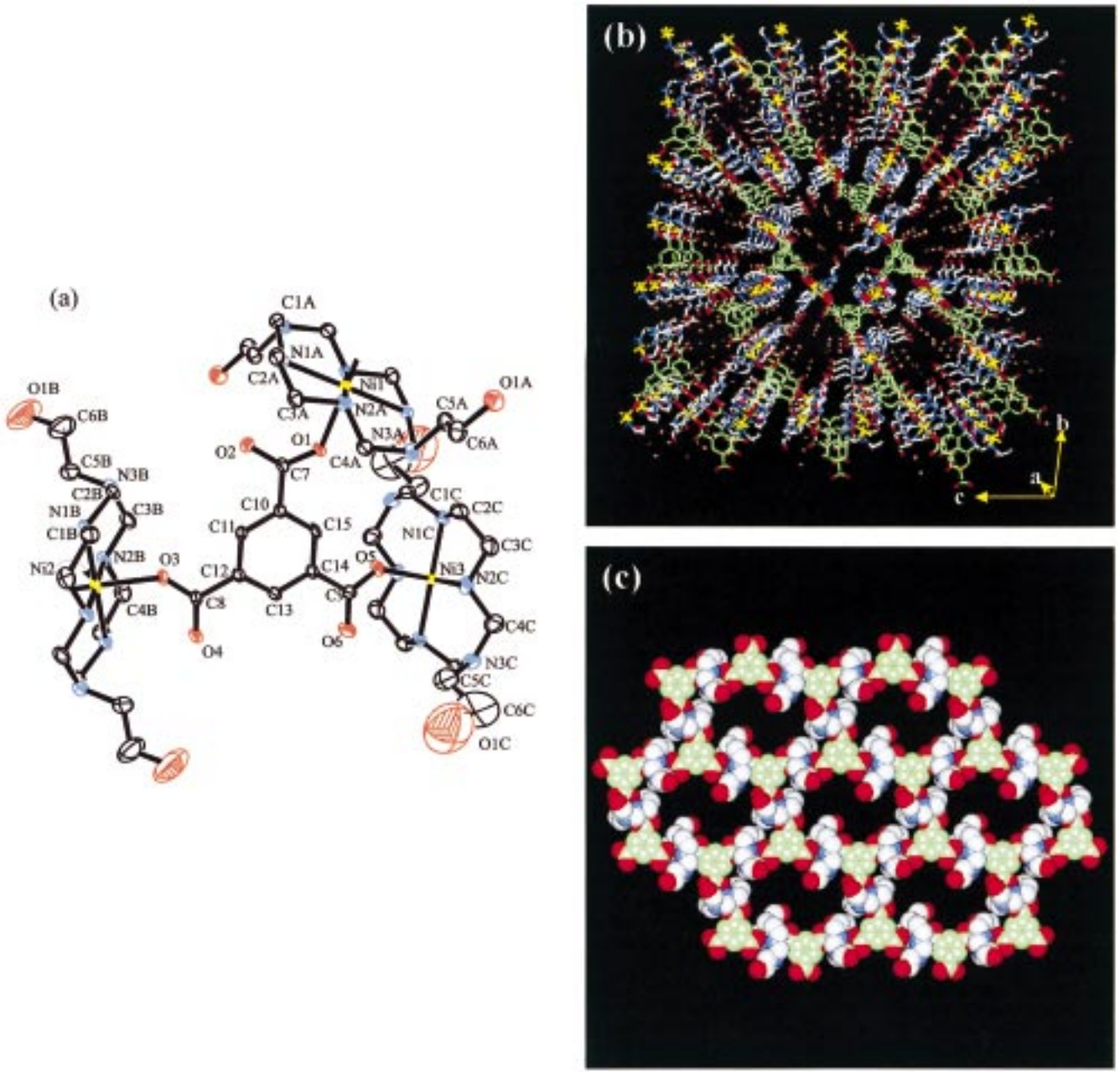

Figure 1. (a) ORTEP view of the trinuclear unit of **1** with atomic numbering scheme. The atoms are represented by 30% probable thermal ellipsoids. (b) Projection of **1** along *a* axis, showing the stacked layers of the molecular brick wall. (c) CPK presentation of the 2-D layer of **1** (yellow, Ni(II) ion; red, oxygen; blue, nitrogen; gray, carbon of macrocycle; green, carbon of BTC^{3-}; pink; oxygen of guest water).

in which two apices of a honeycomb ring become flattened due to the asymmetric binding mode of BTC^{3-} (Figure 1b). The rings are extended along [111] direction to form a 2-D layer of molecular brick wall. The bricks are sheared to an angle of 78.8°. The layers are stacked in parallel, separated by 8.850 Å, with the closest metal−metal distance through the sheets being 9.792 Å. The aromatic rings of the layers are slightly offset-stacked so that the angle between the line perpendicular to the 2-D layer and the line connecting the aromatic rings of the stacked layers becomes 25.3°. This leaves the channels running parallel to *a* axis. The effective void size of the rectangular ring is 6.7 × 13 Å as measured by the distance between van der Waals surfaces of opposing macrocyclic walls (Figure 1c). The cavities are filled with guest molecules, 18 water molecules per unit cell. The network is reinforced with the hydrogen bonding. Within a layer, free carbonyl oxygen atoms of BTC^{3-} form hydrogen bonds with secondary amine hydrogen atoms of the macrocycle (O6- - -N1C#6, 2.871 Å; O4- - -N1B#7, 2.898 Å; O2- -N1A, 2.929 Å; O- -H−N, 150−153°).[33] Due to the hydrogen bonds, the uncoordinated C═O bond distances of BTC^{3-} range 1.232−1.266 Å, which are comparable to the coordinated C−O bond distances of 1.257−1.261 Å. Between the layers, the hydroxyl pendants of the macrocycle located in a layer act as the hydrogen acceptors to form hydrogen bonds with the secondary amines of the macrocycle positioned at the other layer (O1A- - -N2A#1, 2.969 Å; O- -H−N, 152°).[33] The water molecules included in the cavities also form hydrogen bonds with hydroxyl pendants of the macrocycle (O1A- - -OW5#1, 2.787 Å), with carboxylate oxygen atoms (O6- - -OW8#2, 2.648 Å; O4- - -OW6#2, 2.681 Å; O2- - -OW1#3, 2.825 Å), and with the other water inclusions

(33) Symmetry transformations used to generate equivalent atoms: #1, $-x+1, -y, -z$; #2, $x-1, y-1, z$; #3, $x-1, y, z$; #4 $x+1, y, z$; #5, $-x+1, -y+1, -z$; #6, $-x-1, -y-1, -z$; #7, $-x-1, -y, -z+1$.

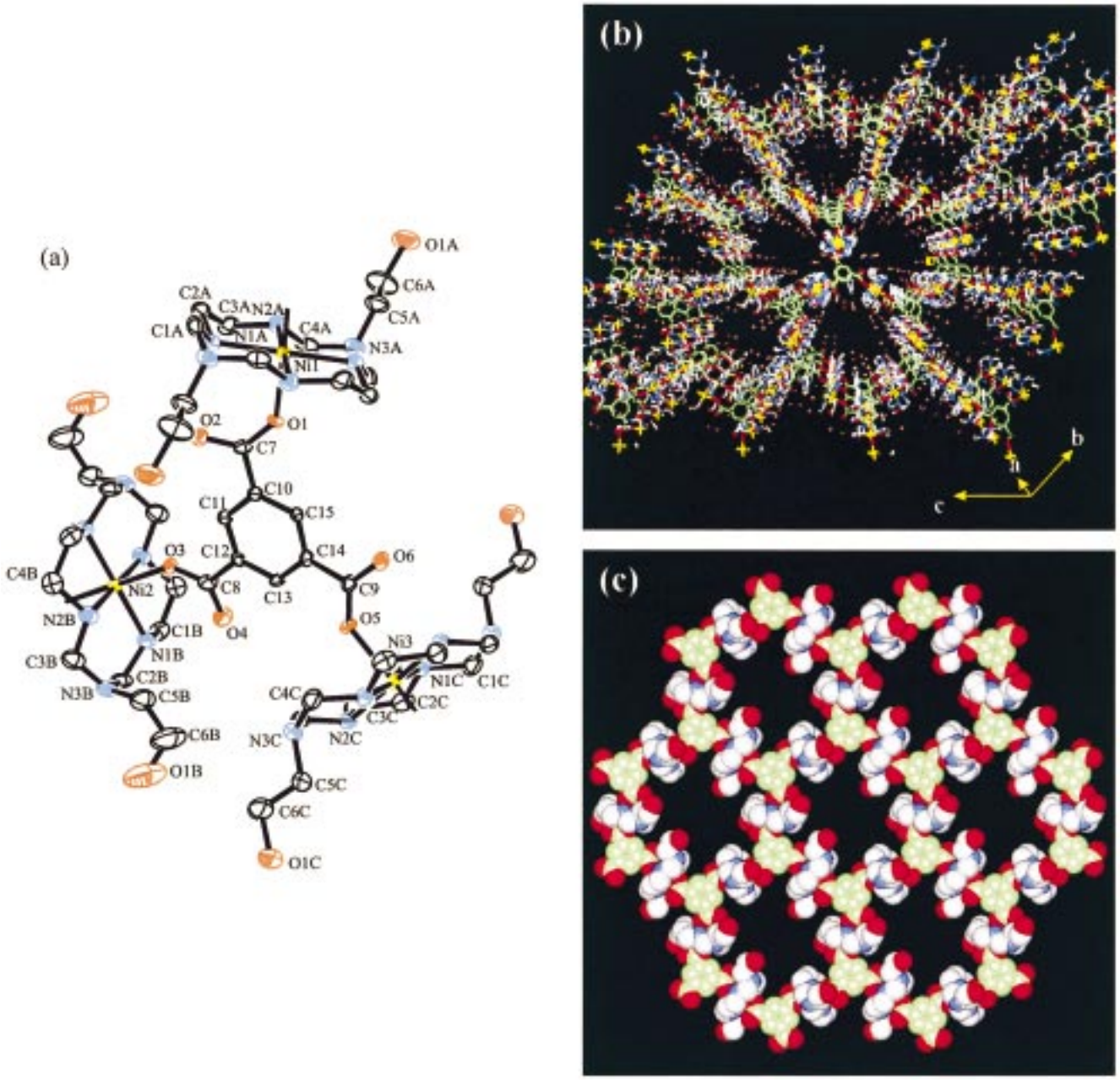

Figure 2. (a) ORTEP view of the trinuclear unit of **2** with atomic numbering scheme. The atoms are represented by 30% probable thermal ellipsoids. (b) Projection of **2** along *a* axis, showing the stacked layers of the molecular honeycomb. (c) CPK presentaion of the 2-D layer of **2** (yellow, Ni(II) ion; red, oxygen; blue, nitrogen; gray, carbon of macrocycle; green, carbon of BTC^{3-}; pink; oxygen of guest water).

(OW6- - -OW8, 2.804 Å; OW1- - -OW4#4, 2.823 Å; OW1- - -OW9#4, 2.650 Å, OW4- - -OW7#5, 2.743 Å).[33]

Guest Inclusion of Molecular Brick Wall 1. To evaluate the framework rigidity of **1**, the absorption of guests was examined by FT-IR spectra and elemental analysis. The experiments were done by immersing large crystals of **1** in benzene, toluene, pyridine, DMF, MeOH, and benzyl alcohol for 12 h. In nonpolar aromatic solvents such as benzene and toluene, the crystals were found to preserve their morphology and only water content in the solid was increased without solvent inclusion. This may be attributed to the hydrophobicity of these solvents, which enhances the hydrogen-bonding interactions between the water inclusions and consequently makes **1** absorb impurity water contained in the solvents. In MeOH, however, the crystals were immediately changed to powder. The analysis of the filtered sample indicated that the water content in the solid was decreased. This is probably due to the dehydration of the cavity water by MeOH. In pyridine, DMF, or benzyl alcohol, the solvent was included in the solid, accompanied with the change of the crystallinity of **1** into powder and the decrease of the included water content. We have obtained crystals of the molecular honeycomb **2** by the reassembly of **1** in the mixture of water and pyridine. The crystal contains pyridine and water molecules as guests. This structure may not be the same as that of simple pyridine inclusion into **1**.

X-ray Crystal Structure of Molecular Honeycomb 2. The fundamental building unit of **2** is shown in Figure 2a. In contrast to **1**, BTC^{3-} coordinates three Ni(II) macrocyclic units by maintaining C_3 rotational symmetry. Therefore, the metal−metal separations around BTC^{3-} become rather symmetrical: Ni1- - -Ni3 = 10.072(1), Ni1- - -Ni2 = 10.056(1), and Ni2- - -Ni3 = 9.802(1) Å. The average Ni−N and Ni−O bond distances are 2.054(3) and 2.132(3) Å, respectively. The dihedral angles between the benzene plane of BTC^{3-} and three

macrocyclic coordination planes involving Ni1, Ni2, and Ni3 ions are 81.8(3), 59.5(2), and 62.7(3)°, respectively. Similarly to **1**, the honeycomb network consists of large rings each of which are made of six Ni(II) macrocycles and six BTC^{3-}. The 2-D layer propagates along the [111] direction. The layers are stacked in parallel by separating 8.973 Å, similarly to **1** (Figure 2b). The nearest metal−metal distance between the sheets is 9.952(1) Å. The aromatic rings of the layers are slightly offset-stacked with an angle of 25.6°, and thus, the hexagonal channels run parallel to the *a* axis. The effective cavity size is ca. 11.4 Å in diameter as measured by the distance between van der Waals surfaces of opposing macrocyclic walls. The cavities are filled with guests, 14 water and two pyridine molecules per unit cell. Each pyridine molecule locates between the benzene rings of BTC^{3-} ions of the adjacent layers. The nearest distance between the pyridine and the benzene rings is 3.64 Å, and the dihedral angle between the benzene ring of BTC^{3-} and the pyridine plane is 61.1°. These indicate the existence of $\pi-\pi$ interaction[34] between the included pyridine and benzene rings of BTC^{3-} ions. The network is reinforced by the hydrogen bonds, similarly to **1**. In the layer, the free carbonyl oxygens of BTC^{3-} form hydrogen bonds with the secondary amines of the macrocycle (O2- - -N1A, 2.969 Å; O4- - -N1B, 2.901 Å; O6#6- - -N2C, 2.966 Å).[33] This is reflected in the uncoordinated C═O bond distances (1.237−1.272 Å) of BTC^{3-}, which are comparable to the coordinated C−O bond distances (1.242−1.266 Å). Between the layers, the hydroxyl pendants of the macrocycle in a layer form hydrogen bonds with the secondary amines of the macrocycle located in the neighboring layers (O1A- - -N2A#1, 3.018 Å; O- -H−N, 114°).[35] The water molecules included in the cavities also involve in the hydrogen bonding with hydroxyl pendants of macrocyclic complex (O1A- - -OW4#1, 2.744 Å; O1B- - -OW6#2, 2.761 Å; O1B- - -OW7#3, 2.784 Å; O1C- - -OW1#2, 2.801 Å; O1C- - -OW2#4, 2.845 Å) and with the carboxylate oxygen atoms (O2- - -OW5, 2.721 Å; O2- - -OW3#2, 2.864 Å; O4- - -OW1, 2.734 Å; O6- - -OW4#5, 2.764 Å) as well as with other cavity water molecules (OW1- - -OW6, 2.816 Å).[35]

Properties. The supramolecular networks of **1** and **2** are insoluble in all solvents except water. The powder diffuse reflectance spectra show maximum absorptions at 504 and 652 nm for **1** and at 505 and 647 nm for **2**, which are the characteristic chromophores for the Ni(II) ion coordinated with N_4O_2 donors.[36] In water, however, both networks decompose into the building blocks, which was identified by the UV/vis spectra showing the characteristic chromophore (λ_{max} = 446 nm) of the starting material **3**.[28]

Molecular-based materials that are stable even after removal of guest molecules are very important in view of the development of a new class of porous substances. However, the crystals of **1** and **2** easily lose their crystallinity by losing some of the water inclusions upon exposure to the atmosphere, which was examined with an optical microscope at ambient temperature. TGA and DTA of the crystalline sample of **1** showed the loss of all guest water molecules at 90 °C and no chemical decomposition up to 190 °C. In the case of **2**, stepwise loss of guests was observed, loss of all water guests at 58 °C and then all pyridine inclusions at 120 °C. No chemical decomposition was observed up to 200 °C. The X-ray powder diffraction patterns of **1** and **2** that were heated at 120 °C for 2 h showed different line positions and intensities as compared with those of the unheated samples, although the patterns indicated the existence of crystallinity. This implies that the distance between the layers is not preserved upon loss of the guest molecules.

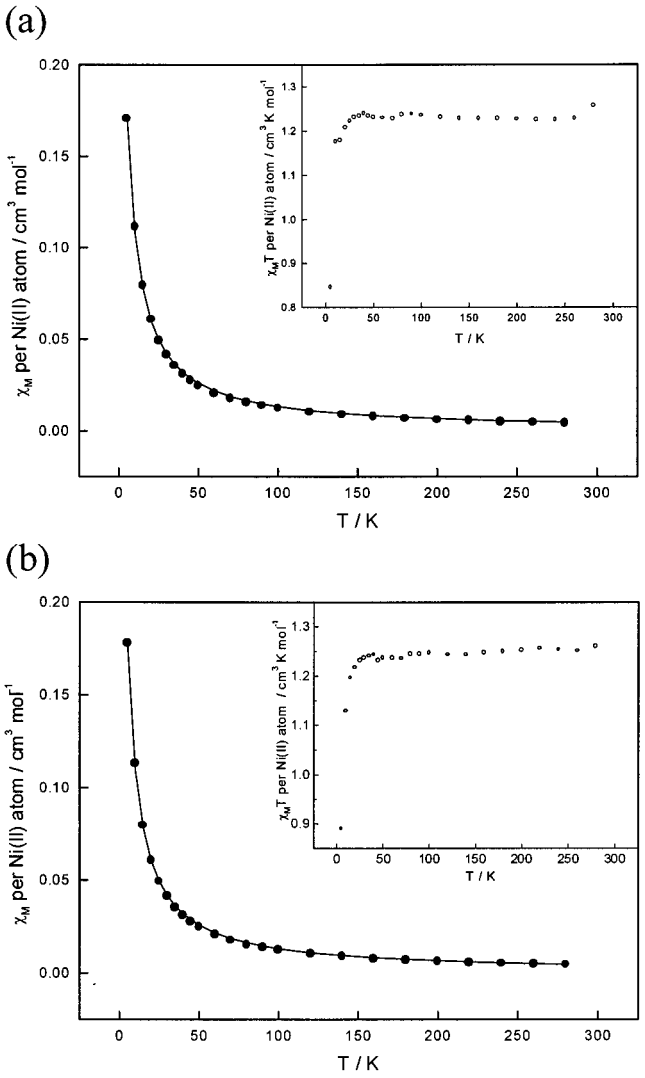

Figure 3. Plots of χ_M vs T and $\chi_M T$ vs T (insert) for **1** (a) and **2** (b). The solid lines represent the best-fit curves to eq 2.

Magnetic Properties. Since the coordination geometry of Ni(II) ion is changed from square-planar to octahedral by the self-assembly, the networks of the molecular brick wall **1** and the molecular honeycomb **2** contain many $S = 1$ paramagnetic centers. We examined the magnetic interaction between these metal centers by measuring the magnetic susceptibility at 2−300 K on a SQUID magnetometer. Figure 3 shows the plots of χ_M vs T and $\chi_M T$ vs T. The χ_M data are interpreted with the isotropic Ni(II) chain spin Hamiltonian described in eq 1 and fitted to eq 2 by neglecting zero-field splitting and the Haldane gap effect.[37,38]

(34) (a) Desiraju, G. R. *Crystal Engineering: the Design of Organic Solids*; Elsevier: New York, 1989; Chapter 4. (b) Brancato-Buentello, K. E.; Scheidt, W. R. *Angew. Chem., Int. Ed. Engl.* **1997**, *36*, 1456. (c) Kimura, E.; Ikeda, T.; Shionoya, M.; Shiro, M. *Angew. Chem., Int. Ed. Engl.* **1995**, *34*, 663.

(35) Symmetry transformations used to generate equivalent atoms: #1, $-x, -y+1, -z$; #2, $x+1, y, z$; #3, $-x+2, -y+1, -z+1$; #4, $x+1, y-1, z$; #5, $-x+1, -y+1, -z$; #6, $-x+2, -y, -z$.

(36) Urbach, F. L. In *Coordination Chemistry of Macrocyclic Compounds*; Melson, G. A., Ed.; Plenum Press: New York, 1979; pp 350−355.

(37) Kahn, O. *Molecular Magnetism*; VCH Publishers: Weinheim, Germany, 1993; Chapter 11, pp 251−263.

(38) Oshio, H.; Okamoto, H.; Kikuchi, T.; Ito, T. *Inorg. Chem.* **1997**, *36*, 3201.

$$H_{\text{chain}} = -J\sum_{i=1}^{n-1} S_i \cdot S_{i+1} \quad (1)$$

$$\chi_{\text{M}} = \frac{N\beta^2 g^2 S(S+1)}{3kT}\frac{1+u}{1-u} \quad (2)$$

$$u = \coth\left[\frac{JS(S+1)}{kT}\right] - \left[\frac{kT}{JS(S+1)}\right]$$

The best-fit parameters are $g = 2.32$ and $J = -1.22$ cm^{-1} for **1** and $g = 2.32$ and $J = -1.08$ cm^{-1} for **2**. This indicates that the paramagnetic Ni(II) centers of the molecular brick wall and the molecular honeycomb weakly couple antiferromagnetically through the BTC^{3-} bridges.

Conclusion. The results demonstrate that $S = 0$ Ni(II) macrocyclic complex can be utilized as a metal building block in the construction of multidimensional networks and the host structures assembled are greatly affected by the guests, even by a partial change of the guests. Although the networks in the present study cannot maintain their three-dimensional frameworks after removal of the included guests, we can apply these results to design supramolecular solids capable of reversible binding of guests.

Acknowledgment. This work was supported by the Korea Science and Engineering Foundation (96-0501-03-01-3) and the Center for Molecular Catalysis.

Supporting Information Available: Tables S1−S12 listing complete crystallographic details, fractional atomic coordinates, anisotropic displacement parameters, interatomic distances and angles, hydrogen atom positions, and bond distances and angles involving hydrogen atoms for **1** and **2** and Figures S1−S7 representing TGA and DTA plots, the X-ray powder diffraction patterns, and the side views showing guest inclusions and interlayer hydrogen-bonding interactions for **1** and **2** (32 pages, print/PDF). An X-ray crystallographic file, in CIF format, is available through the Internet only. See any current masthead page for ordering information and Web access instructions.

JA980504L